Saudi Pharmaceutical Journal 28 (2020) 1616–1625

Contents lists available at ScienceDirect

Saudi Pharmaceutical Journal

journal homepage: www.sciencedirect.com

Original article

Mannose receptor targeted bioadhesive chitosan nanoparticles of clofazimine for effective therapy of tuberculosis

Datta Maroti Pawde [a], Matte Kasi Viswanadh [a], Abhishesh Kumar Mehata [a], Roshan Sonkar [a], Narendra [a], Suruchi Poddar [b], Ankita Sanjay Burande [a], Abhishek Jha [a], Kiran Yellappa Vajanthri [b], Sanjeev Kumar Mahto [b], V.N. Azger Dustakeer [c], Madaswamy S. Muthu [a,*]

[a] Department of Pharmaceutical Engineering and Technology, Indian Institute of Technology (BHU), Varanasi 221005, India
[b] School of Biomedical Engineering, Indian Institute of Technology (BHU), Varanasi 221005, India
[c] Department of Bacteriology, National Institute for Research in Tuberculosis, Chetpet, Chennai 600031, India

ARTICLE INFO

Article history:
Received 31 May 2020
Revised 4 October 2020
Accepted 18 October 2020
Available online 24 October 2020

Keywords:
Chitosan
Clofazimine
Mannose receptor
Nanoparticles
Tuberculosis

ABSTRACT

Drug-resistant tuberculosis (TB) is one of the most lethal diseases, and it is imperative to exploit an advanced drug formulation for its effective treatment. This work aims to develop a mannose receptor-targeted bioadhesive chitosan nanoparticles for effective drug-resistant tuberculosis treatment. The clofazimine loaded chitosan nanoparticles were formulated; their size, charge, polydispersity (PDI), surface morphology, entrapment efficiency (EE) and *in-vitro* release pattern were established. Also, cellular uptake study on C2C12 cell lines and anti-mycobacterial activity against H37Rv (a standard strain of *Mycobacterium tuberculosis*) were evaluated. The particle sizes of formulated chitosan nanoparticles were in the range of 132–184 nm and EE was also found to be between 73 and 95%. The functionalization of bioadhesive chitosan nanoparticles with mannose was confirmed by infrared spectroscopy (FTIR). The uptake studies on the C2C12 cell lines showed that mannosylated nanoparticles were more efficiently internalized when compared to non-targeted nanoparticles. Further, luciferase reporter phage (LRP) assay against H37Rv strain showed that clofazimine nanoparticles were found to be 49.5 times superior in terms of inhibition and anti-mycobacterial activity than free clofazimine. This excellent activity might be attributed to enhanced drug delivery with a promising bioadhesion property of chitosan-based nanoparticles.

1. Introduction

Tuberculosis (TB) is a global plague and a severe health problem throughout the world. It is reported that TB has a lead role in causing the death of people among all highly contagious diseases affecting humans. As reported by the WHO, 9 million of active TB cases are emerging and leading to 2 million deaths each year. Also, TB had a significant impact on human health due to reduced efficacy and less therapeutic effect with mycobacterial chemotherapy (Kaur et al., 2016, Reshma et al., 2017). The possible reasons behind this are drug degradation before reaching the intended target site, sub-optimal drug concentrations reaching the infection site, insufficient permeation of medication into macrophages as well as granulomas which are the reservoirs that house dormant bacteria within the alveolar tissue of the host. It is quite challenging to treat the mycobacterial infections too, as mycobacteria are notoriously resistant intracellular pathogens (Pinheiro et al., 2011). About 33% of the human population in the world is infected with latent TB, among which chances of transformation into active TB are 5–10% (Reshma et al., 2017). Global strategies for controlling TB include directly observed therapy short-course (DOTS) for efficient management of TB. Even though DOTS is a beneficial treatment method, it is a comparatively costlier treatment strategy and has many other functional challenges, mostly in emerging nations. The highly efficient treatment system is therefore required, which reduces the duration of medication and the risk of relapse. This allows scientists to design advanced drug delivery systems to amplify the treatment for TB that is therapeutically successful at the clinical level (Kaur et al., 2016).

* Corresponding author.
E-mail address: muthubits@rediffmail.com (M.S. Muthu).

Peer review under responsibility of King Saud University.

Production and hosting by Elsevier

https://doi.org/10.1016/j.jsps.2020.10.008
1319-0164/

To bridge the requirements of anti-tubercular therapy, various nanomedicine-based drug delivery systems have been designed to eliminate the problems related to the drugs. Recently, various nanosystems such as liposomes, nanoparticles, and micelles, etc. have been utilized to deliver therapeutics in the treatment of TB (Agrawal and Gupta, 2000, Gaspar et al., 2008). Nano drug delivery systems have several potential advantages compared with the conventional medicines for tuberculosis therapy, including higher payload capacity, enhanced permeability and retention effect, sustained blood circulation times, diminished toxicity to healthy tissues and improved efficacy (Agrawal et al., 2017, Mehata et al., 2020). Clofazimine (Cfz) is a riminophenazine antibiotic that is lipophilic and enjoys both antimycobacterial as well as anti-inflammatory activities. This drug shows activity against *Mycobacterium tuberculosis* (MTB) including its multidrug-resistant (MDR) strains. It is suggested as a Group 5 medicine by WHO for use in patients with extensively drug-resistant tuberculosis (XDR-TB) (Cholo et al., 2012). Also, Cfz is highly permeable and is classified as the Biopharmaceutics Classification System (BCS) class II drug. It has minimal solubility in aqueous systems; hence the efficacy of Cfz is limited (Li et al., 2017).

Chitosan is a natural, positively charged biocompatible polysaccharide polymer. It has many useful properties such as biodegradability, nontoxic, low immunogenicity and also possesses antibacterial properties. The cationic nature has made chitosan more beneficial for cell surface adhesion and enables substantial crosslinking with polyvalent ionic compounds. The bioadhesive property enables the prolonged retention of chitosan-based nanoformulations on to the targeted substrate (Agrawal et al., 2017, Duceppe and Tabrizian, 2010). FDA recently recommends D-alpha tocopheryl polyethylene glycol 1000 succinate (TPGS) as a safe additive and extensively used as a stabilizer, solubility, absorption and penetration enhancer while formulating drug delivery systems for hydrophobic drugs(Duceppe and Tabrizian, 2010, Zhang et al., 2012). TPGS is suitable for use in nanoformulations because of its amphiphilic property (emulsifier) and can overcome multidrug resistance as it is an inhibitor of P-gp efflux pump (Kutty et al., 2015). Recently, the use of an efflux pump inhibitor as a powerful approach to shortening TB treatment and killing drug-tolerant bacteria was successfully tested (Szumowski et al., 2013, Mustafa et al., 2017). Therefore, TPGS could be an ideal constituent to formulate nanoparticles for tuberculosis targeting. Recently, Gaspar et al. have established that passively targeted nanoformulations loaded with antitubercular drugs were preferably cumulated in the hepatocytes and spleen following i.v. injection, rather than in the lungs which could be a promising approach for extra-pulmonary TB treatment (Gaspar et al., 2008). In another study, El-Ridy et al. formulated a passively targeted nanomedicine loaded with pyrazinamide and it was administered through i.v. route in mice. With a total of seven treatment doses and injected two days a week, this nanomedicine efficiently decreased the MTB bacilli count when compared to the non-formulated drug at a similar dose and frequency (El-Ridy et al., 2007). Although this kind of passively targeted nanomedicine may not possess high sensitivity/ specificity/ efficacy for the TB therapy, decoration of targeting moiety on the surface can improve their targetability and efficiency.

The mannose receptor (MR) family is identified in rabbit alveolar macrophages which are recognized by glycosylated lysosomal enzyme, mannose, N-acetylglucosamine and fucose (Wileman et al., 1986, Weis et al., 1998, Shepherd et al., 1981, Largent et al., 1984). The role of MR in immunity is to safeguard the host in the initial period of the disease, which is primarily acquired by phagocyting the microorganisms mediated by the expression of the MR cDNA, as shown in COS-1 cells. The MR receptor has an affinity to a wide variety of micro-organisms such as *Pneumocystis carinii*, *Candida albicans*, *Mycobacterium tuberculosis* and *Leishmania donovani* and *Klebsiella pneumonia* which frequently express mannose and N-acetylglucosamine on the glycoproteins that decorate these micro-organisms (Ezekowitz et al., 1990, Ezekowitz et al., 1991, Chakraborty and Das, 1988, Schlesinger, 1993). In general, macrophages contain mannose receptors on their outer layer that can recognize and bind with the non-reducing terminal of mannose moiety and thus facilitate cellular uptake of nanoparticles (Kumar et al., 2006, Praphakar et al., 2018, Vieira et al., 2017). Therefore, the mannosylated nanoformulation may be an effective strategy for targeting macrophages of alveoli by the active delivery of therapeutics for targeted TB therapy. The decoration of mannose on a drug delivery vehicle has facilitated a higher uptake of these carriers by macrophage leading to better activity and minimal side effects, which may be correlated to the preferential and selective absorption of mannose by macrophages of alveoli leading to selective accumulation of drug-loaded nanoparticles within the targets (Hirota et al., 2007, Kumar et al., 2006, Verma et al., 2008).

Therefore, the present study aims to develop and characterize TPGS emulsified, targeted bioadhesive nanoparticles for the delivery of Cfz to the macrophages of lung's alveoli where the etiological organism of TB is mainly present. The bioadhesive nanoparticles of chitosan were primarily designed to actively deliver Cfz to the alveolar macrophages by surface modification with mannose.

2. Materials and methods

2.1. Materials

Chitosan (extra pure) and D-mannose were procured from SRL, Mumbai, India. Spectrum laboratories Inc., U.S.A supplied the 1 kDa molecular weight cut off dialysis membrane. Clofazimine (Cfz), sodium tripolyphosphate, coumarin-6 (CM6) and chloroform were brought from Sigma-Aldrich Chemicals Pvt Ltd, India. Antares Health Products., U.S.A supplied PEGylated vit E (TPGS) as a gift sample. The C2C12 cell line was obtained from National Centre for Cell Science, Pune, India. Other reagents used in this research were of analytical quality.

2.2. Methods

2.2.1. Preparation of Cfz/CM-6 loaded bioadhesive chitosan nanoparticles

The solvent evaporation method with slight modification and with the utilization of the ionic cross-linking principle was utilized to formulate the different nanoparticles (NPs) (Ren et al., 2010). For the preparation of Cfz loaded chitosan NPs (Cfz-CS-NP), 0.2% CH3COOH solution was used to dissolve 30 mg of chitosan and pH was made up to 6.0 using 0.1 N NaOH solution. Later, 20 mg TPGS and 3 mg Cfz was dissolved in 1 ml of chloroform and transferred to the above mixture and probe-sonicated to form nanoemulsion. The nanoemulsion was evaporated by stirring for 12 h, followed by adding 2.5 ml of sodium tripolyphosphate (TPP) solution having a concentration of 2 mg/ml to induce crosslinking. The larger particles and unentrapped drug crystals were then eliminated by centrifugation at a speed of 4000 rpm for 15 min. After removing unwanted particles, centrifugation was done at a speed of 17,000 rpm for 15 min, and the supernatant, free from particulate matter, was eliminated and the settled NPs were rinsed three times with purified distilled water to separate any unentrapped drug from the exterior of the NPs. The resulting NPs were then dispersed in distilled water by gentle shaking on a vortexer. The Cfz loaded targeted NPs (Cfz-CS-MNS-NP) were also made by the same method with some modifications. In targeted nanoparticles, mannose decoration to the surface was achieved with a 2 ml mannose solution (10 mg, pH 4) followed by addition

to the Cfz loaded non-targeted formulation (Cfz-CS-NP) and gently stirring for 48 h. According to literature, the mannose molecules would undergo the ring-opening reaction due to the acidic environment and the aldehyde moiety would then interact with the free amino group located on the exterior of the chitosan, resulting in a Schiff 's base (—N═CH—). Further, targeted NPs (Cfz-CS-MNS-NP) were dialyzed by using a dialysis membrane (1 kDa) for 30 min with double distilled water in the receptor compartment to remove uncoated mannose and other impurities (Vieira et al., 2017, Jiang et al., 2008). The CM6 loaded non-targeted (CM6-CS-NP) and targeted NPs (CM6-CS-MNS-NP) were formulated in the same way by replacing Cfz by CM6 (0.3 mg) (Fig. 1 and Table 1) (Guo et al., 2014).

2.2.2. Nanoparticles characterization

2.2.2.1. Characterization of chitosan-mannose conjugation. The lyophilized NPs were analyzed by infrared spectroscopy (FTIR) to find Schiff 's base and to confirm the mannose coating over the NPs. The FTIR was performed with Bruker, Massachusetts, U.S.A installed with an attenuated total reflectance (ATR) device with a zinc selenite crystalline sample holder. The lyophilized NPs were placed on the attenuated total reflectance chamber and scanned 32 times, and an average result was generated. The samples were scanned between wavenumber 4000–600 cm^{-1}, and the spectra were obtained with a resolution of 4 cm^{-1}.

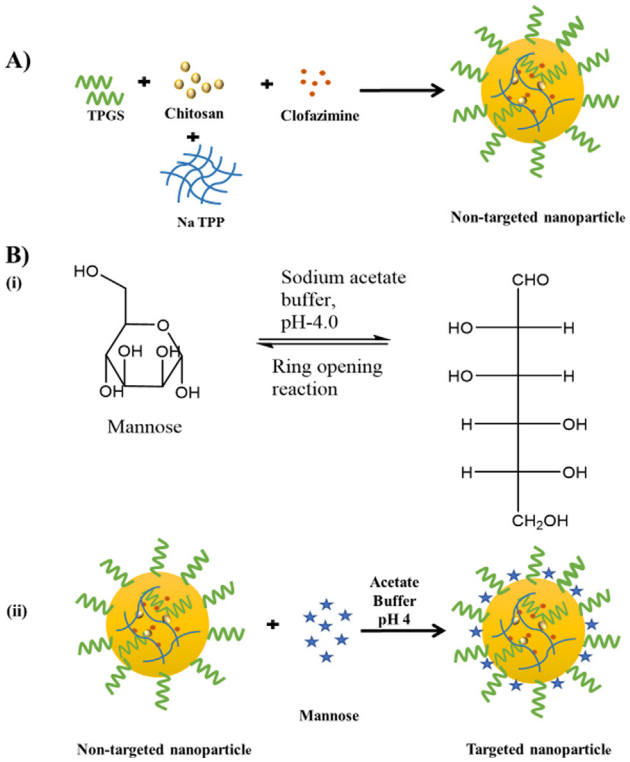

Fig. 1. Schematic diagram for (A) preparation of non-targeted nanoparticles (Cfz-CS-NP) and B) (i) mannose ring opening reaction and (ii) preparation of targeted nanoparticles (Cfz-CS-MNS–NP).

2.2.2.2. Dynamic light scattering (DLS). Particle size, including polydispersity index and zeta potential of all the formulations were analyzed by DLS (Zetasizer, Nano-S90, Malvern) at room temperature. By using purified distilled water, nanoformulations were diluted up to four times and then passed through a 0.22 μm syringe filter (Millipore). The zeta potential of the samples was measured based on the principle of electrophoretic mobility properties of nanoparticles when placed in the electric field. All the results reported were the average of 3 successive individual measurements (n = 3) (Mehata et al., 2019).

2.2.2.3. Scanning electron microscopy (SEM). The SEM (ZEISS Supra 40, Germany) was utilized for the visualizing of surface characteristics of Cfz-CS-NP and Cfz-CS-MNS-NP. The SEM was set at 20 kV, was utilized for scanning the samples. The samples were visualized after two times dilution with double distilled water, spread uniformly on glass slides followed by drying in a vacuum tray dryer. The pictures were collected with a magnification of 40,000× (Agrawal et al., 2017).

2.2.2.4. Transmission electron microscopy (TEM). The prepared NPs, i.e., Cfz-CS-NP and Cfz-CS-MNS-NP were evaluated by TEM (Philips CM-12., Fullerton, CA, U.S.A) for visualization of surface morphology. The samples were diluted ten times with purified distilled water, and a drop of each nanoformulations was kept on a carbon-coated TEM grid and drying was achieved under vacuum pressure. The pictures were taken at 80,000 V with a TEM (Mehata et al., 2019).

2.2.2.5. Atomic force microscopy (AFM). The formulated nanoparticles were visualized under AFM (Solver P-47-PRO, MDT; Moscow, Russia) to obtain the surface texture of formulated NPs. AFM was brought in tapping operation mode and utilizing high resonance frequency (F0 = 241 kHz), pyramidal cantilevers with silicon probes were used with force constants of around 41 N/m. The samples were diluted up to ten times with purified distilled water; one drop of diluted sample was spread evenly on a coverslip and dried in a vacuum drier at 25 °C for 24 h. At 2 Hz scan speeds AFM images were captured and by using AFM image analysis software (Solver P-47-PRO), the height measurements were obtained (Agrawal et al., 2017).

2.2.2.6. Estimation of entrapment efficiency (EE). In short, at 10,000 rpm, 1 ml of NPs suspension was centrifuged, and the supernatant was eliminated, the sediment was re-dispersed into

Table 1
Formulation of bioadhesive NPs.

Batches	Chitosan (mg)	TPGS (mg)	Mannose (mg)	Cfz (mg)	CM6 (mg)	Sodium TPP (2 mg/ml)
CS-NP	30	20	–	–	–	2.5
Cfz-CS-NP	30	20	–	3	–	2.5
Cfz-CS-MNS-NP	30	20	10	3	–	2.5
CM6-CS-NP	30	20	–	–	0.3	2.5
CM6-CS-MNS-NP	30	20	10	–	0.3	2.5

CS-NP: TPGS emulsified chitosan nanoparticles.
Cfz-CS-NP: Cfz loaded TPGS emulsified chitosan nanoparticles.
Cfz-CS-MNS-NP: Cfz loaded mannose receptor targeted nanoparticles.
CM6-CS-NP: CM6 loaded chitosan nanoparticles.
CM6-CS-MNS-NP: CM6 loaded mannose receptor targeted nanoparticles.

1 ml of purified distilled water. A 0.2 ml of the above suspension was evaporated under vacuum pressure at 35 °C to dryness in a rotary evaporator. The residue was dissolved in methanol (10 ml) with the aid of bathsonicator for ensuring complete breakage of nanoparticles to release the entrapped Cfz and get solubilized into methanol. The sample was centrifuged at 10,000 rpm for 10 min. The collected supernatant was processed through a 0.45 μm syringe filter. Finally, the absorbance was obtained using a spectrophotometer at 491 nm (Shimadzu 1800, Tokyo, Japan). The linear standard calibration data of Cfz measured in methanol was found to be in the range of 2–10 μg/ml with R^2 value 0.999. According to the definition, drug EE can be calculated by taking the ratio of the amount of Cfz entrapped within the nanoparticles to the total Cfz added in the nanoparticle fabrication.

The EE of Cfz was determined as

$$\text{Cfz EE } (\%) = \frac{\text{Amount of Cfz loaded within nanoparticles}}{\text{The total amount of Cfz added during the preparation}} \times 100$$

The EE of CM6 loaded within the NPs was estimated by fleorometry. In brief, 1 ml of NPs suspension, i.e., CM6-CS-NP and CM6-CS-MNS-NP were centrifuged at 17 k rpm for 10 min, and after discarding the supernatant, the settled NPs were re-suspended in 1 ml purified water. A 0.2 ml of the above suspension was evaporated under vacuum pressure at 35 °C to dryness in a rotary evaporator. Further centrifugation was performed to the obtained solution for 10 min at 10 k rpm, and the resulting supernatant after centrifugation was taken out and passed through a 0.45 μm syringe filter. From above, 0.5 ml was taken, and it was made up to 4 ml. For the CM6 excitation wavelength (462 nm) and emission wavelengths (502 nm) were set in the fluorimeter, and the readings of samples were noted. The calibration curve obtained for CM6 in chloroform was found to be linear within the range 5–50 ng/ml with an R^2 value of 0.999. The EE of CM6 loaded nanoparticles was determined similarly as it has been used for the estimation of Cfz (Agrawal et al., 2017; Mehata et al., 2019).

2.2.3. In-vitro evaluation

2.2.3.1. In-vitro Cfz release studies. The dynamic dialysis process was utilized to observe the release of Cfz from Cfz-CS-NP, Cfz-CS-MNS-NPs (Feng et al., 2018). A 1 ml of NPs sample (containing 0.3 mg of Cfz) was centrifuged at a speed of 10,000 rpm for 10 min, and the upper portion of aliquot was discarded accompanied by rinsing of settled NPs with purified distilled water to exclude the free Cfz. After washing, the NPs were suspended in 1 ml purified water and loaded into the dialysis bag (regenerated cellulose membrane, 1 kDa), adequately sealed and placed in 50 ml PBS (pH 7.4) in a beaker with 0.2% v/v DMSO. The complete system was held at 37 ± 0.5 °C, with continuous shaking at 100 rpm/min in a water bath shaker. Then, at predetermined time intervals, 5 ml aliquots were removed from the receptor compartment and replenished with fresh buffer medium to maintain sink condition. Using 0.45 μm syringe filters, the samples were filtered and the drug content was estimated with the help of a UV spectrophotometer. The profile of the *in-vitro* drug release was constructed by plotting the graph between % release and time (Chaves et al., 2018).

2.2.3.2. In-vitro qualitative cellular uptake study. C2C12 cells (1×10^4 viable cells) were seeded on 22 mm^2 cover slips plated on petri dishes in DMEM and incubated for 1209-10at 37 °C in the presence of 5% CO_2. Thus, prepared monolayer of cells was further incubated for 12 h at 37 °C in the presence of 5% CO_2 with different formulations i.e., plain CM6, CM6-CS-NP and CM6-CS-MNS-NP in equivalent quantity of CM6 (5 μg/ml). The washing of cells was performed after 2 h of incubation with pH 7.4 PBS, followed by fixing with 4% paraformaldehyde for 10 min. The washing of cells was again performed three times with pH 7.4 PBS and the staining of nuclei was done by incubating with 100 μl of DAPI at a concentration of 0.1 μg/ml for 10 min. Finally, the cell monolayer was further washed three times with pH 7.4 PBS and cover glasses were then mounted and observed by an inverted fluorescence microscope (Nikon Ti-U and NIS- elements software) (Mehata et al., 2019; Muthu et al., 2015).

2.2.4. In-vitro antibacterial activity

2.2.4.1. Luciferase reporter phage (LRP) assay. The preparation of cell suspension was performed by inoculating the exponential phase culture of *M. tuberculosis* from LJ medium slope, which was corresponding to #1 MacFarland standard units into G7H9 broth within Bijou bottles and vortexed with a few glass beads. The antimycobacterial activity of Cfz (aqueous suspension in Tween 80), Cfz-CS-NP and Cfz-CS-MNS-NP were studied by harnessing LRP assay as depicted by Sivakumar et al., with some changes. Approximately 350 μl of G7H9 broth, enriched with 0.5% glycerol and 10% albumin-dextrose complex, was measured in cryovials and supplemented with 50 μl of crude extract to obtain the required concentration. All sample vials were supplemented with 100 μl *M. tuberculosis* cell suspension and 1% of DMSO was used as solvent control in this analysis. After the addition of treatments, incubation was done at 37 °C for all the vials for 72 h, following incubation, 50 μl of high titer mycobacteriophage phAETRC202 and 40 μl of $CaCl_2$ (0.1 M) was transferred to both test and control vials. All sample vials were subjected for incubation at 37 °C for 4 h and an aliquot of 100 μl, after incubation, transferred to the cuvette of the luminometer from all sample vials. With the addition of 100 μl of D-Luciferin, the relative light unit (RLU) was estimated in a luminometer (Monolight 2010) (Dusthackeer et al., 2008). The RLU % reduction was calculated as

$$RLU\% = \frac{Control\ \ RLU - Test\ \ RLU}{Control\ \ RLU} \times 100$$

2.2.5. Statistical analysis

The obtained data were calculated as a mean of three measurements (n = 3 ± S.D). Average values of such distinct characteristics were compared using the analysis of variance (ANOVA) as size, entrapment, and various *in-vitro* data. Differences are deemed to be statistically significant at a P value < 0.05.

3. Results and discussion

3.1. Characterization of chitosan-mannose conjugation

FTIR spectra of chitosan, mannose, non-targeted and targeted NP formulations were correlated in Fig. 2. A peak at 3393.86 cm^{-1} demonstrated the existence of primary amine and —OH functional group stretching vibrations in chitosan. A distinct —NH— bending at 1518.33 cm^{-1} confirmed the amine functionalities of chitosan in the formulation of Cfz-CS-NP for attaching the mannose. The functionalization process was made by the ring-opening reaction of the mannose and then the reaction of its —CHO group with —NH_2 group (free) situated on the surface of Cfz-CS-NP. It results in the formation of Schiff's base (R—CH═N—R) that was indeed confirmed by the appearance of —NH— bending related to secondary amines at 1547.41 cm^{-1} and C═N stretch at 1394.14 cm^{-1}. Moreover, the shift of the peak of Cfz-CS-NP from 2927.15 cm^{-1} to 2986.60 cm^{-1} and its broadening in Cfz-CS-MNS-NP supported the formation of chitosan-mannose conjugate (Chaubey and Mishra, 2014).

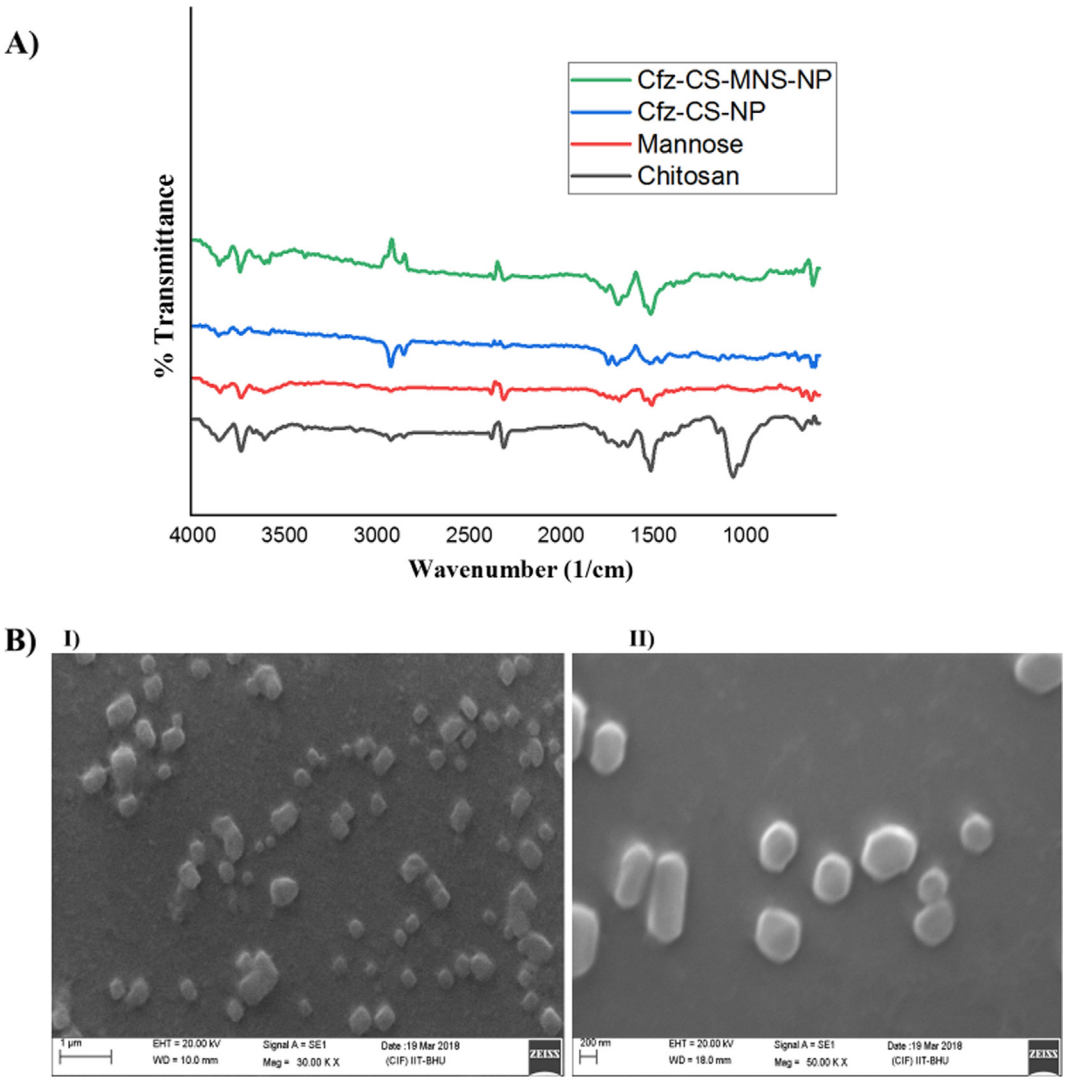

Fig. 2. A) FTIR spectra of chitosan, mannose, Cfz-CS-NP, Cfz-CS-MNS-NP and B) SEM images of batches I) Cfz-CS-NP, II) Cfz-CS-MNS-NP.

3.2. Dynamic light scattering (DLS)

Table 2 demonstrated the average particle size and polydispersity index (PDI) of Cfz and CM6 loaded NPs. The Cfz loaded and CM6 loaded non-targeted and targeted formulations shown the mean size in the range of 132.8 ± 2.30, 184.7 ± 2.37, 134.7 ± 0.55 and 182.9 ± 0.73 nm, respectively. Also, size measurements indicated that the prepared NPs were in the 100–200 nm size range. It was observed that targeting ligand (mannose) decoration on the surface of mannose receptor targeted NPs led to a notable increment in particle size. The PDI of all the formulations demonstrated that the prepared NPs have quite a compact size distribution, i.e., near about 0.3. The batch Cfz-CS-NP showed more positive zeta potential; however the conjugation of mannose on the surface of targeted NPs has led to the lowering of the positive charge (Table 2).

3.3. Scanning electron microscopy (SEM)

The SEM pictures of different batches are depicted in Fig. 2. In the obtained pictures, prepared nanoparticles were almost cubic to round in morphological structures with more or less size range of around 200 nm. The images also reveal the even surface of particles with the absence of notable pinholes or fissures. The obtained images further suggested that mannose conjugation onto the surface has increased the particle size of targeted NPs (Agrawal et al., 2017).

3.4. Transmission electron microscopy

Using TEM, external morphological features of prepared NPs were observed and these studies demonstrated that prepared NPs have spherical morphology (Fig. 3A). The particle size as seen by TEM in Fig. 3A, was correlated with results obtained from DLS and SEM, which were comparable and were in good agreement.

3.5. Atomic force microscopy

The AFM scans of each of Cfz-CS-NP, Cfz-CS-MNS-NPs were shown in Fig. 3B (I to IV). The particles were found to have spherical morphology with absence of any visible pinholes or fractures. It was also revealed that the images of mannose conjugated NPs were more or less round in morphological structure and with the particle size of <190 nm.

3.6. EE of NPs

The amount of Cfz or CM6 loading in the different nanoparticles were calculated by comparing the obtained absorbance or fluroscence reading against their standard calibration curve. The Cfz or

Table 2
Particle size, polydispersity index, zeta potential and entrapment efficiency.

Batches	Particle size (mean ± S.D[a]) (nm)	Polydispersity (mean ± S.D[a])	Zeta potential (mean ± S.D[a]) (mV)	Entrapment efficiency (%) (mean ± S.D[a])
Cfz	–	–	–	–
CS-NP	126.7 ± 1.21	0.31 ± 0.030	13.05 ± 0.02	–
Cfz-CS-NP	132.8 ± 2.30	0.32 ± 0.013	12.05 ± 0.01	94.86 ± 0.55
Cfz-CS-MNS-NP	184.7 ± 2.37	0.33 ± 0.017	9.12 ± 0.08	73.45 ± 1.47
CM6-CS-NP	134.7 ± 0.55	0.23 ± 0.023	4.13 ± 0.05	92.88 ± 0.64
CM6-CS-MNS-NP	182.9 ± 0.73	0.26 ± 0.014	2.19 ± 0.12	87.27 ± 0.90

n = 3.
S.D[a]: Standard deviation.
Cfz: Clofazimine pure drug.
CS-NP: TPGS emulsified chitosan nanoparticles.
Cfz-CS-NP: Cfz loaded TPGS emulsified chitosan nanoparticles.
Cfz-CS-MNS-NP: Cfz loaded mannose receptor targeted nanoparticles.
CM6-CS-NP: CM6 loaded chitosan nanoparticles.
CM6-CS-MNS-NP: CM6 loaded mannose receptor targeted nanoparticles.

CM6 loading was found to be 2.85 mg, 2.20 mg, 0.28 mg and 0.26 mg for Cfz-CS-NP, Cfz-CS-MNS-NP, CM6-CS-NP and CM6-CS-MNS-NP, respectively. Based on the drug loading data of different nanoparticles, their EE was calculated. The EE can be stated as the % ratio of the amount of Cfz present in NPs in comparison to that of the quantity of Cfz used during the formulation of nanoparticles. In this study, drug EE in Cfz-CS-NP and Cfz-CS-MNS-NP was found to be 94.86 ± 0.55% and 73.45 ± 1.47%, respectively (Table 2). The EE for the nanoparticles prepared with CM6 in CM6-CS-NP and CM6-CS-MNS-NP was found to be 92.88 ± 0.64%, 87.27 ± 0.90%, respectively (Table 2).

3.7. In-vitro studies

3.7.1. In-vitro drug release studies

The *in-vitro* drug release pattern of the drug from Cfz-CS-NP and Cfz-CS-MNS-NP in PBS (pH 7.4) (resembling the environment physiological pH) are shown in Fig. 4A. The Cfz loaded non-targeted and targeted NPs showed release continuously for >36 h without any signs of burst release. The extent of drug release was calculated to be 85.58% for Cfz-CS-NP and 70.98% for Cfz-CS-MNS-NP, respectively after performing the *in-vitro* release of Cfz for 72 h in PBS pH 7.4 (Nagpal et al., 2013).

3.7.2. In-vitro qualitative cellular uptake

The uptake of NPs by cells was proposed as a two-step fashion, firstly by the adhering of NPs to the cell surface, and secondly, the cellular engulfment. Using fluorescence microscopy, the fluorescence from CM6 loaded non-targeted and targeted NPs or pure C6 was seen in C2C12 cells. The pure CM6, CM6-CS-NP and the CM6-CS-MNS-NP, with 5 μg/ml equivalent of CM6, were incubated with the cells then counterstained with DAPI to observe the nucleus. The green fluorescence was obtained from the FITC filter, which demonstrated the distribution of CM6 loaded nanoformulation and pure CM6 inside the cells. In this study, CM6-CS-MNS-NP exhibited relatively higher green fluorescence in the C2C12 cells. Within the cytoplasm, they produced more green stain in comparison to the pure CM6 as well as CM6-CS-NP, which can be seen in Fig. 4B. The images revealed that very little fluorescence was exhibited by the pure CM6 in comparison to CM6-CS-NP and CM6-CS-MNS-NP. Indeed, due to the mannose receptor-mediated endocytosis and bioadhesive nature, uptake of targeted nanoparticles into the cytoplasm of C2C12 cells was higher (Vijayakumar et al., 2016).

3.7.3. Antibacterial activities

3.7.3.1. LRP assay. The Cfz loaded non-targeted nanoparticles and targeted nanoparticles showed percentage inhibition of 98% and 99% respectively; the percentage inhibition was significantly higher when compared to the free Cfz (i.e., only 2%) (Fig. 5). In comparison to free Cfz, a significant reduction in percentage inhibition values was observed for Cfz-CS-NP and Cfz-CS-MNS-NP. It might be attributed to the enhanced uptake of Cfz loaded nanoparticles across the mycobacterial membrane, which results in maximum drug involvement in the inhibition activities. However, there is no significant reduction in percentage inhibition values between non-targeted and targeted NPs due to the non-availability of the mannose receptor on *M. tuberculosis*. The superior outcome represents that Cfz loaded nanoparticles may act as an efficient drug delivery system for antimycobacterial activity.

4. Discussion

Targeted drug delivery system offers numerous advantages over conventional drug delivery systems that includes delivering of drug to desired site, reduction in the dose and minimization of the peripheral toxicity (Edgar and Wang, 2017). Here, in this study we have presented targeted nanoparticles based on chitosan for effective targeting of lung's alveoli macrophages where the etiological organism of TB is mainly present and prepared nanoparticles were evaluated for various parameters.

FTIR is the one of simple and best method for identification of functional groups, their modification and conjugates formed via interaction of the functional groups. Each compound has their own unique finger print in the FTIR spectra that helps in the identification of the compounds. In this study, we have used chitosan as a polymeric drug carrier, whose FTIR spectra demonstrated a peak at 3393.86 cm^{-1} that represents the presence of primary amine and —OH functional group in the chitosan. Additionally, significantly well identified peak at 1518.33 cm^{-1} represented the —NH— bending of the free amine group in the Cfz-CS-NP. Further, conjugation of the mannose on to the surface of the nanoparticles, demonstrated a peak at 2986.60 cm^{-1} of the Cfz-CS-MNS-NP. These obtained FTIR results were well correlated with the reported values in the literature (Chaubey and Mishra, 2014).

With the help of DLS analysis, it was found that Cfz-CS-NP and Cfz-CS-MNS-NP have the particle size of 132.8 ± 2.30 nm and 184.7 ± 2.37 nm respectively, whereas CM6-CS-NP and CM6-CS-MNS-NP were found to have the particle size of 134.7 ± 0.55 nm and 182.9 ± 0.73 nm. Surface functionalization of the mannose on to the nanoparticles slightly increases the particle sizes of the nanoparticles. Nanoparticles can affect the pharmacokinetics and biodistribution of the loaded drugs that has significant role in the *in-vivo* therapeutic applications (Alexis et al., 2008). Hence, the size and surface properties of the nanoparticles deemed to have key importance in the drug delivery. The nanoparticles greater than

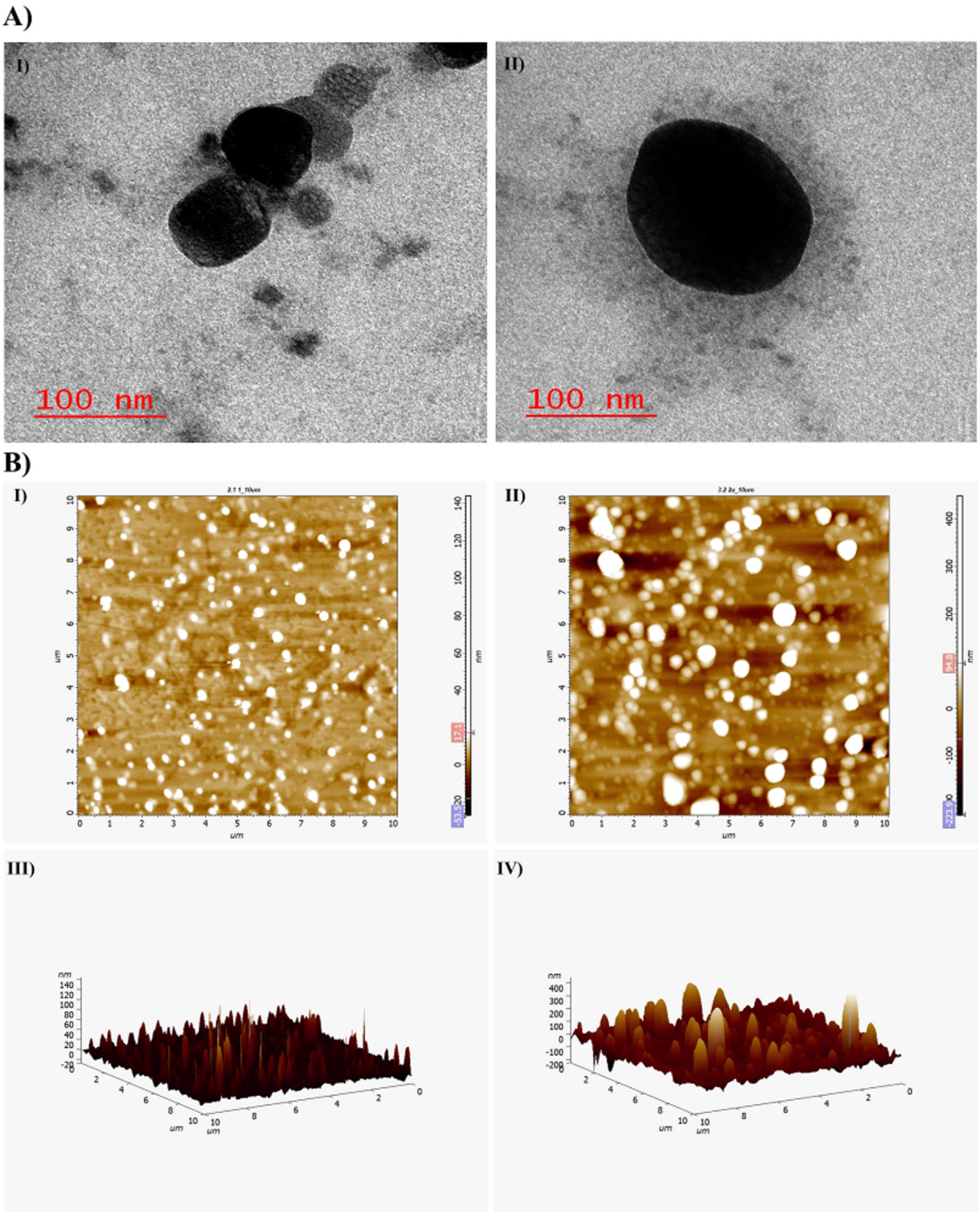

Fig. 3. A) TEM images of I) Cfz-CS-NP, II) Cfz-CS-MNS-NP and B) 2D AFM images of I) Cfz-CS-NP, II) Cfz-CS-MNS-NP; 3D AFM images of III) Cfz-CS-NP, IV) Cfz-CS-MNS-NP.

100 nm are effectively uptake by Kupffer or other reticuloendothelial system phagocytes and constrain their distribution to undesired site of the body (Pratten and Lloyd, 1986). Moreover, surface functionalization of the mannose decreases the zeta potential of the nanoparticle that was mainly due to the reduction of the primary amine group of the chitosan, which was utilized for the formation of bond with CHO group of the mannose.

The surface morphology studies were performed with the help for SEM, TEM, and AFM. The images obtained from SEM were observed to have spherical to cubic morphology and some of the found to be in rod shape, may be due to end to end aggregation of the nanoparticles (Fig. 2B). Additionally, TEM analysis confirmed that the prepared nanoparticles were having spherical morphology with the size below 200 nm, which was well correlation with the

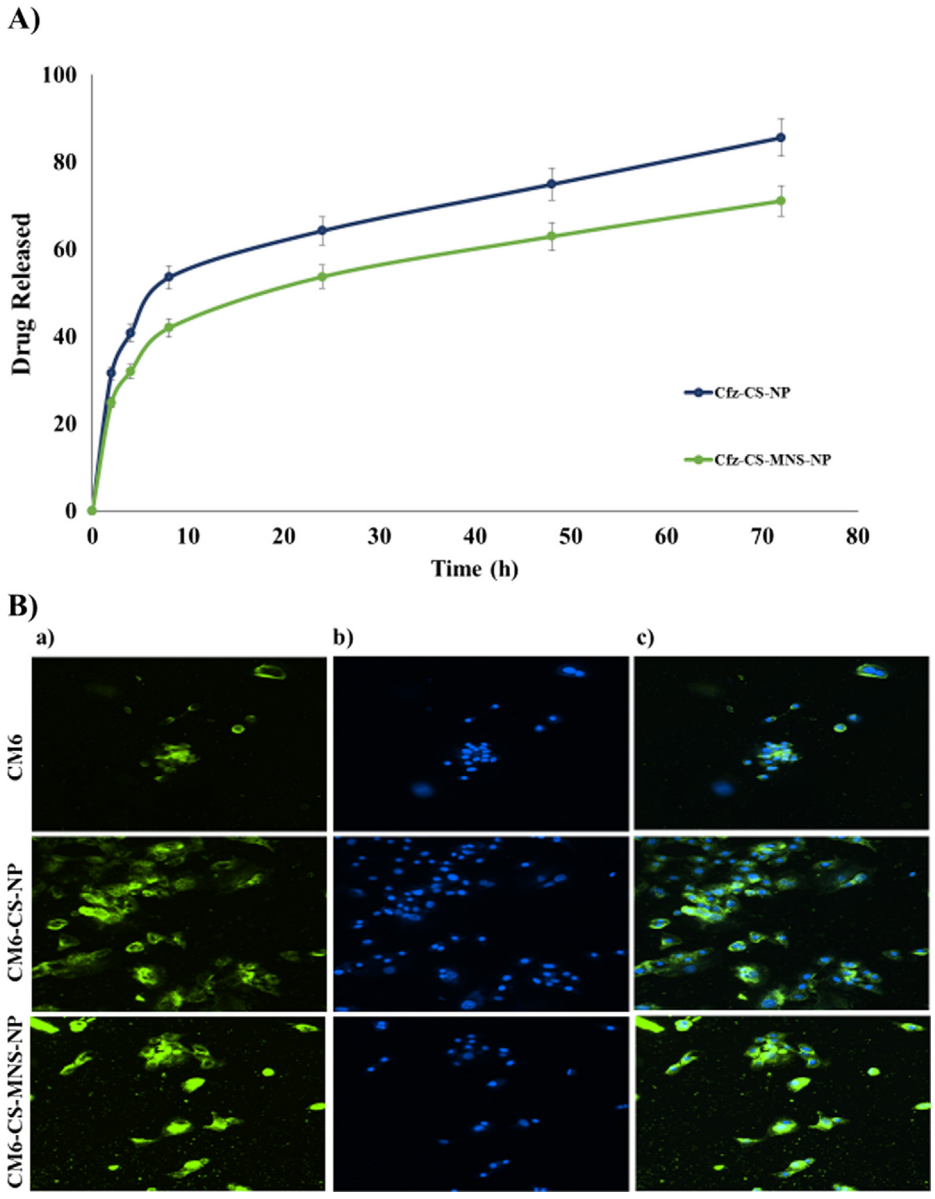

Fig. 4. A) *In-vitro* release study of non-targeted (Cfz-CS-NP) and targeted nanoparticles (Cfz-CS-MNS-NP) in PBS (pH 7.4); B) The microscopy images of C2C12 cells after 2 h incubation with free CM6, CM6-CS-NP and CM6-CS-MNS-NP. (a) FITC filter, (b) DAPI filter, (c) superimposed image captured through both the FITC and DAPI filters.

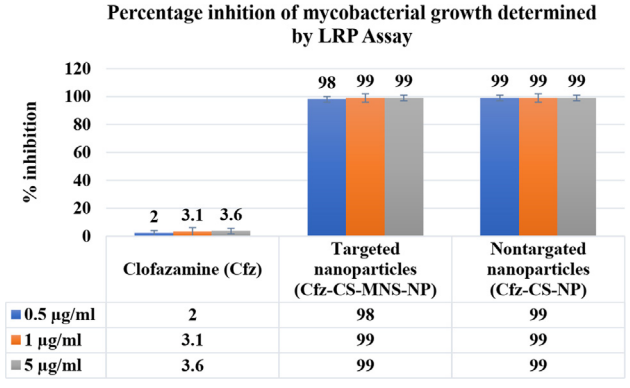

	Clofazamine (Cfz)	Targeted nanoparticles (Cfz-CS-MNS-NP)	Nontargated nanoparticles (Cfz-CS-NP)
0.5 µg/ml	2	98	99
1 µg/ml	3.1	99	99
5 µg/ml	3.6	99	99

Fig. 5. Antimycobacterial Activity against *M. tuberculosis* H37Rv by luciferase reporter phage (LRP) assay.

data obtained from DLS. Further, TEM images demonstrated mannose conjugation on to the surface of nanoparticles modified the surface morphology (Cfz-CS-MNS-NP) with significant increment in the particle size (Fig. 3A). The AFM analysis further supported the above statements.

The EE of drug in the nanoparticles can be calculated by the direct and indirect methods. In the indirect method, free drug is analysed in the supernatant phase of nanoparticles obtained after centrifugation (Daneshmand et al., 2018). In this study, we have estimated EE by direct method that represents analyzing the drug that is present inside the nanoparticles. The EE of Cfz in Cfz-CS-NP and Cfz-CS-MNS-NP was observed to be 94.86 ± 0.55% and 73.45 ± 1.47%, respectively. Whereas for CM6 loaded CM6-CS-NP and CM6-CS-MNS-NP was observed to have 92.88 ± 0.64%, 87.27 ± 0.90% of EE, respectively. The prepared nanoparticles seem to have significant % EE, which indicate that minimal wastage of the drug

may occur during the formulation of nanoparticles because greater portion of drug is entrapped inside nanoparticles.

The *in-vitro* release study of Cfz from Cfz-CS-NP and Cfz-CS-MNS-NP was performed in phosphate buffer saline of pH 7.4 that represent the physiological pH environment of the body. It was noted that 30–40% of drug was released in first 5 h, which may be due to release of drug that adhered onto nanoparticles surfaces or release of the drug present just below the nanoparticle surfaces. Sustained release of Cfz were from Cfz-CS-NP and Cfz-CS-MNS-NP observed in 10 h to 72 h, which represent the diffusion of Cfz from the core of nanoparticles towards its surface and then into the buffer media. Moreover, sustain release of Cfz from nanoparticles can be also be correlated with the insoluble nature of chitosan at pH 7.4. Finally, at 72 h % release of Cfz from Cfz-CS-NP and Cfz-CS-MNS-NP was found to be 85.58% and 70.98%, respectively (Chaubey and Mishra, 2014).

The cellular uptake study of nanoparticles of indicated the efficiency of the prepared nanoparticles to internalize in the targeted cells (Asthana et al., 2014). If, we look inside the mechanism of the nanoparticles cellular uptake, it is a two-step process, firstly by the adhering of NPs to the cell surfaces, and secondly, the cellular engulfment (schematically represented in Fig. 6). In this study we have taken CM6, a highly sensitive fluorescent dye that can be easily observed under fluoroscent microscope, for preparation of CM6-CS-NP and the CM6-CS-MNS-NP. It was maily due to the non-fluroscent nanture of the Cfz that can not be observed under fluroscent microscope. *In-vitro* cellular uptake study demostrated that CM6-CS-MNS-NP have relatively higher green fluorescence in the cytoplasm of the C2C12 cells, in comparision to the CM6 and CM6-CS-NP (Fig. 4B). CM6 has poor aqueous solubility that limits its permeabilty across cellular membrane of the C2C12 cells. Although, CM6 is entrapped inside CM6-CS-NP, their cellular uptake occurs by passive transport mechnism. Whereas in CM6-CS-MNS-NP, due to the mannose receptor-mediated endocytosis and bioadhesive nature, uptake into the cytoplasm of C2C12 cells was higher.

LPR assay is one of the most efficient testing methods for detection, identification, and antibiotic susceptibility testing of *M. tuberculosis*. In this study, it was found that Cfz-CS-NP and Cfz-CS-MNS-NP have the percentage inhibition of 98% and 99% respectively, whereas free Cfz was found to have the percentage inhibition of only 2%. This can be correlated with the higher cellular uptake of Cfz-CS-NP and Cfz-CS-MNS-NP, relative to Cfz. Further, there was no any significant difference between percentage inhibition of Cfz-CS-NP and Cfz-CS-MNS-NP observed due to the non-availability of the mannose receptor on *M. tuberculosis* (Dusthackeer et al., 2008).

5. Conclusion

In this study, we tried to develop the mannose receptor targeted bioadhesive chitosan NPs. The prepared NPs were further surface conjugated with mannose that facilitates receptor guided drug delivery to mycobacterium infected macrophages. The prepared nanoparticle formulations were characterized for physio-chemical parameters and *in-vitro* activity. The data obtained from DLS were observed to be acceptable. The Cfz EE of mannose receptor targeted NPs and non-targeted NPs was observed to be 94.86 ± 0.55% and 73.45 ± 1.47%, respectively. The CM6 EE of CM6-CS-NP and CM6-CS-MNS-NP was observed to be 79% and 73%. 92.88 ± 0.64% and 87.27 ± 0.90%, respectively. The *in-vitro* drug release at pH 7.4 was found to be slow and sustained. Uptake studies showed that mannosylated nanoparticles (CM6-CS-MNS-NP) were

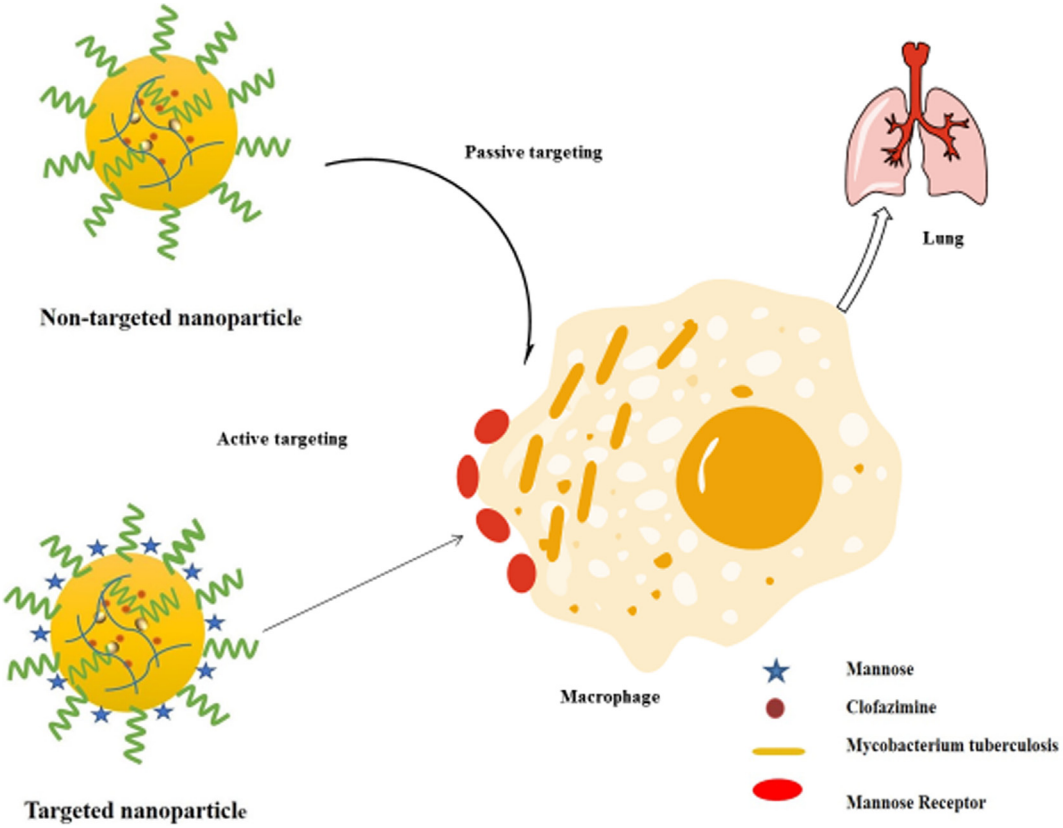

Fig. 6. Schematic diagram for uptake mechanism of mannose receptor targeted chitosan nanoparticles.

more efficiently internalized when compared to CM6-CS-NP and free CM6 (Fig. 4B). Further, the LRP assay against *M. tuberculosis* H37Rv (standard strain *M. tuberculosis*) showed that Cfz loaded nanoparticles have 49.5 times higher inhibition efficiency than free Cfz suspension. After regulatory validation, these nanoparticles may be clinically used to target the mycobacterium infected macrophages for the active therapy of drug-resistant tuberculosis.

Declaration of Competing Interest

The authors declare that reported data in the manuscript have no conflict of interest.

Acknowledgements

The authors acknowledge the Indian Institute of Technology (BHU), Varanasi, India, for the Research Support Grant (2017-2018) to facilitate nanomedicine based targeted drug delivery research, and for providing Ministry of Education (MoE), Government of India Scholarship.

References

Agrawal, A.K., Gupta, C.M., 2000. Tuftsin-bearing liposomes in treatment of macrophage-based infections. Adv. Drug Deliv. Rev. 41, 135–146.
Agrawal, P., Singh, R.P., Sonali, Kumari, L., Sharma, G., Koch, B., Rajesh, C.V., Mehata, A.K., Singh, S., Pandey, B.L., Muthu, M.S., 2017. TPGS-chitosan cross-linked targeted nanoparticles for effective brain cancer therapy. Mater. Sci. Eng. C Mater. Biol. Appl. 74, 167–176.
Alexis, F., Pridgen, E., Molnar, L.K., Farokhzad, O.C., 2008. Factors affecting the clearance and biodistribution of polymeric nanoparticles. Mol. Pharm. 5, 505–515.
Asthana, G.S., Asthana, A., Kohli, D.V., Vyas, S.P., 2014. Mannosylated chitosan nanoparticles for delivery of antisense oligonucleotides for macrophage targeting. Biomed. Res. Int. 2014, 526391.
Chakraborty, P., Das, P.K., 1988. Role of mannose/N-acetylglucosamine receptors in blood clearance and cellular attachment of Leishmania donovani. Mol. Biochem. Parasitol. 28, 55–62.
Chaubey, P., Mishra, B., 2014. Mannose-conjugated chitosan nanoparticles loaded with rifampicin for the treatment of visceral leishmaniasis. Carbohydr. Polym. 101, 1101–1108.
Chaves, L.L., Costa Lima, S.A., Vieira, A.C.C., Barreiros, L., Segundo, M.A., Ferreira, D., Sarmento, B., Reis, S., 2018. Development of PLGA nanoparticles loaded with clofazimine for oral delivery: Assessment of formulation variables and intestinal permeability. Eur. J. Pharm. Sci. 112, 28–37.
Cholo, M.C., Steel, H.C., Fourie, P.B., Germishuizen, W.A., Anderson, R., 2012. Clofazimine: current status and future prospects. J. Antimicrob. Chemother. 67, 290–298.
Daneshmand, S., Golmohammadzadeh, S., Jaafari, M.R., Movaffagh, J., Rezaee, M., Sahebkar, A., Malaekeh-Nikouei, B., 2018. Encapsulation challenges, the substantial issue in solid lipid nanoparticles characterization. J. Cell. Biochem. 119, 4251–4264.
Duceppe, N., Tabrizian, M., 2010. Advances in using chitosan-based nanoparticles for in vitro and *in vivo* drug and gene delivery. Expert Opin. Drug Deliv. 7, 1191–1207.
Dusthackeer, A., Kumar, V., Subbian, S., Sivaramakrishnan, G., Zhu, G., Subramanyam, B., Hassan, S., Nagamaiah, S., Chan, J., Paranji Rama, N., 2008. Construction and evaluation of luciferase reporter phages for the detection of active and non-replicating tubercle bacilli. J. Microbiol. Methods 73, 18–25.
Edgar, J.Y.C., Wang, H., 2017. Introduction for Design of Nanoparticle Based Drug Delivery Systems. Curr. Pharm. Des. 23, 2108–2112.
El-Ridy, M.S., Mostafa, D.M., Shehab, A., Nasr, E.A., Abd El-Alim, S., 2007. Biological evaluation of pyrazinamide liposomes for treatment of Mycobacterium tuberculosis. Int. J. Pharm. 330, 82–88.
Ezekowitz, R.A., Sastry, K., Bailly, P., Warner, A., 1990. Molecular characterization of the human macrophage mannose receptor: demonstration of multiple carbohydrate recognition-like domains and phagocytosis of yeasts in Cos-1 cells. J. Exp. Med. 172, 1785–1794.
Ezekowitz, R.A., Williams, D.J., Koziel, H., Armstrong, M.Y., Warner, A., Richards, F.F., Rose, R.M., 1991. Uptake of Pneumocystis carinii mediated by the macrophage mannose receptor. Nature 351, 155–158.
Feng, J., Zhang, Y., Mcmanus, S.A., Ristroph, K.D., Lu, H.D., Gong, K., White, C.E., Prud'homme, R.K., 2018. Rapid Recovery of Clofazimine-Loaded Nanoparticles with Long-Term Storage Stability as Anti-Cryptosporidium Therapy. ACS Appl. Nano Mater. 1, 2184–2194.
Gaspar, M.M., Cruz, A., Penha, A.F., Reymão, J., Sousa, A.C., Eleutério, C.V., Domingues, S.A., Fraga, A.G., Filho, A.L., Cruz, M.E., Pedrosa, J., 2008. Rifabutin encapsulated in liposomes exhibits increased therapeutic activity in a model of disseminated tuberculosis. Int. J. Antimicrob. Agents 31, 37–45.
Guo, Y., Chu, M., Tan, S., Zhao, S., Liu, H., Otieno, B.O., Yang, X., Xu, C., Zhang, Z., 2014. Chitosan-g-TPGS nanoparticles for anticancer drug delivery and overcoming multidrug resistance. Mol. Pharm. 11, 59–70.
Hirota, K., Hasegawa, T., Hinata, H., Ito, F., Inagawa, H., Kochi, C., Soma, G., Makino, K., Terada, H., 2007. Optimum conditions for efficient phagocytosis of rifampicin-loaded PLGA microspheres by alveolar macrophages. J. Control. Release 119, 69–76.
Jiang, H.-L., Kang, M.L., Quan, J.-S., Kang, S.G., Akaike, T., Yoo, H.S., Cho, C.-S., 2008. The potential of mannosylated chitosan microspheres to target macrophage mannose receptors in an adjuvant-delivery system for intranasal immunization. Biomaterials 29, 1931–1939.
Kaur, R., Garg, T., Malik, B., Gupta, U.D., Gupta, P., Rath, G., Goyal, A.K., 2016. Development and characterization of spray-dried porous nanoaggregates for pulmonary delivery of anti-tubercular drugs. Drug Deliv. 23, 882–887.
Kumar, P.V., Asthana, A., Dutta, T., Jain, N.K., 2006. Intracellular macrophage uptake of rifampicin loaded mannosylated dendrimers. J. Drug Target. 14, 546–556.
Kutty, R.V., Tay, C.Y., Lim, C.S., Feng, S.-S., Leong, D.T.J.N.R., 2015. Anti-migratory and increased cytotoxic effects of novel dual drug-loaded complex hybrid micelles in triple negative breast cancer cells. Nano Res. 8, 2533–2547.
Largent, B.L., Walton, K.M., Hoppe, C.A., Lee, Y.C., Schnaar, R.L., 1984. Carbohydrate-specific adhesion of alveolar macrophages to mannose-derivatized surfaces. J. Biol. Chem. 259, 1764–1769.
Li, H.-Z., Ma, S.-H., Zhang, H.-M., Liu, J.-M., Wu, Y.-X., Cao, P.-Q., Gao, X., 2017. Nano carrier mediated co-delivery of dapsone and clofazimine for improved therapeutic efficacy against tuberculosis in rats. Biomed. Res. 28, 8.
Mehata, A.K., Bharti, S., Singh, P., Viswanadh, M.K., Kumari, L., Agrawal, P., Singh, S., Koch, B., Muthu, M.S., 2019. Trastuzumab decorated TPGS-g-chitosan nanoparticles for targeted breast cancer therapy. Colloids Surf. B Biointerfaces 173, 366–377.
Mehata, A.K., Viswanadh, M.K., Priya, V., Muthu, M.S., 2020. Dendritic cell-targeted theranostic nanomedicine: advanced cancer nanotechnology for diagnosis and therapy. Nanomedicine (Lond) 15, 947–949.
Mustafa, S., Devi, V.K., Pai, R.S., 2017. Kanamycin Sulphate Loaded PLGA-Vitamin-E-TPGS Long Circulating Nanoparticles Using Combined Coating of PEG and Water-Soluble Chitosan. J. Drug Deliv. 2017, 1253294.
Muthu, M.S., Kutty, R.V., Luo, Z., Xie, J., Feng, S.S., 2015. Theranostic vitamin E TPGS micelles of transferrin conjugation for targeted co-delivery of docetaxel and ultra bright gold nanoclusters. Biomaterials 39, 234–248.
Nagpal, K., Singh, S.K., Mishra, D., 2013. Evaluation of safety and efficacy of brain targeted chitosan nanoparticles of minocycline. Int. J. Biol. Macromol. 59, 20–28.
Pinheiro, M., Lúcio, M., Lima, J.L., Reis, S., 2011. Liposomes as drug delivery systems for the treatment of TB. Nanomedicine (Lond) 6, 1413–1428.
Praphakar, R.A., Shakila, H., Dusthackeer, V.N.A., Munusamy, M.A., Kumar, S., Rajan, M.J.P.C., 2018. A mannose-conjugated multi-layered polymeric nanocarrier system for controlled and targeted release on alveolar macrophages. Polym. Chem. 9, 656–667.
Pratten, M.K., Lloyd, J.B., 1986. Pinocytosis and phagocytosis: the effect of size of a particulate substrate on its mode of capture by rat peritoneal macrophages cultured in vitro. BBA 881, 307–313.
Ren, W.-H., Chang, J., Yan, C.-H., Qian, X.-M., Long, L.-X., He, B., Yuan, X.-B., Kang, C.-S., Betbeder, D., Sheng, J., 2010. Development of transferrin functionalized poly (ethylene glycol)/poly (lactic acid) amphiphilic block copolymeric micelles as a potential delivery system targeting brain glioma. J. Mater. Sci. - Mater. Med. 21, 2673–2681.
Reshma, R.S., Jeankumar, V.U., Kapoor, N., Saxena, S., Bobesh, K.A., Vachaspathy, A.R., Kolattukudy, P.E., Sriram, D., 2017. Mycobacterium tuberculosis lysine-ε-aminotransferase a potential target in dormancy: Benzothiazole based inhibitors. Bioorg. Med. Chem. 25, 2761–2771.
Schlesinger, L.S., 1993. Macrophage phagocytosis of virulent but not attenuated strains of Mycobacterium tuberculosis is mediated by mannose receptors in addition to complement receptors. J. Immunol. 150, 2920–2930.
Shepherd, V.L., Lee, Y.C., Schlesinger, P.H., Stahl, P.D., 1981. L-Fucose-terminated glycoconjugates are recognized by pinocytosis receptors on macrophages. Proc. Natl. Acad. Sci. USA 78, 1019–1022.
Szumowski, J.D., Adams, K.N., Edelstein, P.H., Ramakrishnan, L., 2013. Antimicrobial efflux pumps and Mycobacterium tuberculosis drug tolerance: evolutionary considerations. Curr. Top. Microbiol. Immunol. 374, 81–108.
Verma, R.K., Kaur, J., Kumar, K., Yadav, A.B., Misra, A., 2008. Intracellular time course, pharmacokinetics, and biodistribution of isoniazid and rifabutin following pulmonary delivery of inhalable microparticles to mice. Antimicrob. Agents Chemother. 52, 3195–3201.
Vieira, A.C., Magalhães, J., Rocha, S., Cardoso, M.S., Santos, S.G., Borges, M., Pinheiro, M., Reis, S., 2017. Targeted macrophages delivery of rifampicin-loaded lipid nanoparticles to improve tuberculosis treatment. Nanomedicine (Lond) 12, 2721–2736.
Vijayakumar, M.R., Vajanthri, K.Y., Balavigneswaran, C.K., Mahto, S.K., Mishra, N., Muthu, M.S., Singh, S., 2016. Pharmacokinetics, biodistribution, in vitro cytotoxicity and biocompatibility of Vitamin E TPGS coated trans resveratrol liposomes. Colloids Surf. B Biointerfaces 145, 479–491.
Weis, W.I., Taylor, M.E., Drickamer, K., 1998. The C-type lectin superfamily in the immune system. Immunol. Rev. 163, 19–34.
Wileman, T.E., Lennartz, M.R., Stahl, P.D., 1986. Identification of the macrophage mannose receptor as a 175-kDa membrane protein. Proc. Natl. Acad. Sci. USA 83, 2501–2505.
Zhang, Z., Tan, S., Feng, S.S., 2012. Vitamin E TPGS as a molecular biomaterial for drug delivery. Biomaterials 33, 4889–4906.